Available online at www.sciencedirect.com
ScienceDirect
Journal of Sound and Vibration 316 (2008) 234–247
JOURNAL OF SOUND AND VIBRATION
www.elsevier.com/locate/jsvi

# An efficient realization of frequency dependent boundary conditions in an acoustic finite-difference time-domain model

José Escolano[a,b,*], Finn Jacobsen[a], José J. López[b]

[a]*Acoustic Technology, Ørsted.DTU, Technical University of Denmark, Building 352, DK-2800 Kgs. Lyngby, Denmark*
[b]*Institute of Telecommunications and Multimedia Applications, Technical University of Valencia, E-46022 Valencia, Spain*

Received 8 February 2007; received in revised form 20 February 2008; accepted 20 February 2008
Handling Editor: R.J. Astley
Available online 8 April 2008

**Abstract**

The finite-difference time-domain (FDTD) method provides a simple and accurate way of solving initial boundary value problems. However, most acoustic problems involve frequency dependent boundary conditions, and it is not easy to include such boundary conditions in an FDTD model. Although solutions to this problem exist, most of them have high computational costs, and stability cannot always be ensured. In this work, a solution is proposed based on ''mixing modelling strategies''; this involves separating the FDTD mesh and the boundary conditions (a digital filter representation of the impedance) and combining them into a global solution. This solution is based on an interaction model that involves wave digital filters. The proposed method is validated with several test cases.


## 1. Introduction

Numerical calculations of sound fields in complex enclosures must take account of aspects as for example geometric shape and properties of materials. The current power of computers makes it possible to approach the solution of such problems with several methods. One important time-domain method is known as the finite-difference time-domain (FDTD) method [1,2]. This method provides a simple and accurate solution with relatively low computational cost. However, one of its handicaps is that it is fairly complicated to take account of frequency dependent complex impedance boundary conditions, which is important, e.g., in room acoustics [3] and in outdoor sound propagation [4]. A review of time-domain impedance boundary conditions can be found in a paper by Fung and Ju [5].

Most time-domain impedance models are based on a modification of the wave equation at the mesh points where the impedance is situated [6,7]; and to define a general method for any analytical expression for the impedance and ensure its stability is not a simple task. The method presented in this paper combines an FDTD mesh with a digital filter representation of the boundary condition. This combination of simulation methods is

*Corresponding author at: Institute of Telecommunications and Multimedia Applications, Technical University of Valencia, E-46022 Valencia, Spain.
*E-mail addresses:* escolano@ujaen.es (J. Escolano), fja@oersted.dtu.dk (F. Jacobsen), jjlopez@dcom.upv.es (J.J. López).

0022-460X/$ - see front matter © 2008 Elsevier Ltd. All rights reserved.
doi:10.1016/j.jsv.2008.02.035

known in some contexts as "mixing modelling strategies" [8]; this means that a combination of method can improve the entire method. However, as will become clear, this combination cannot be made directly because of stability problems. This will be solved by using a wave digital filter (WDF) as a common interface [9]. For simplicity, the theory presented in this paper is for 2D problems. However, it is straightforward to extend it to 3D.

## 2. FDTD theory

The FDTD method, as first proposed by Yee [10], is a simple and elegant way of discretizing the differential form of Maxwell's equations. In FDTD modelling of wave equations, the space solution is discretized using the "Yee cell", and the vector component of the electrical and magnetic field are distributed around the unit cell so as to allow the differential operators to be approximated by second-order centred finite differences that combine to second-order derivatives. A similar algorithm has been derived for sound fields [11]. Although improved and more accurate FDTD algorithms have been developed for aeroacoustic applications (e.g., based on approximations of higher-order, unstaggered meshes, upwind schemes[12,13]), Yee's staggered algorithm remains an economical and robust way to carry out the FDTD algorithm [14], giving a compromise between accuracy and efficiency. This scheme has been widely used in fields such as room acoustic applications [2,3,15,16], musical sound synthesis [17–19], and outdoor sound propagation [20–22].

In the staggered FDTD in acoustics, the scalar pressure and the three components of the particle velocity are distributed around an acoustic Yee unit cell [11], which is similar to the original electromagnetic FDTD cell, but based on conservation of mass and momentum (see Fig. 1),

$$\frac{\partial p(\mathbf{r},t)}{\partial t} = -\rho_0 c^2 \nabla \cdot \mathbf{u}(\mathbf{r},t), \tag{1}$$

$$\rho_0 \frac{\partial \mathbf{u}(\mathbf{r},t)}{\partial t} = -\nabla p(\mathbf{r},t), \tag{2}$$

where $p$ is the sound pressure, $\mathbf{u}$ is the acoustic particle velocity, $\mathbf{r}$ is the position, $t$ is the time, $c$ is the speed of sound, and $\rho_0$ is the density of air.

The FDTD method studied in this paper uses a second-order central finite-difference approach to the derivatives [23]. In Cartesian coordinates Eqs. (1) and (2) become (in 2D) the following system of discretized equations:

$$p(i,j,n+1) = p(i,j,n) - \frac{\rho_0 c^2 \Delta t}{\Delta x}[u_x(i+\tfrac{1}{2},j,n+\tfrac{1}{2}) - u_x(i-\tfrac{1}{2},j,n+\tfrac{1}{2})] - \frac{\rho_0 c^2 \Delta t}{\Delta y}[u_y(i,j+\tfrac{1}{2},n+\tfrac{1}{2}) - u_y(i,j-\tfrac{1}{2},n+\tfrac{1}{2})], \tag{3}$$

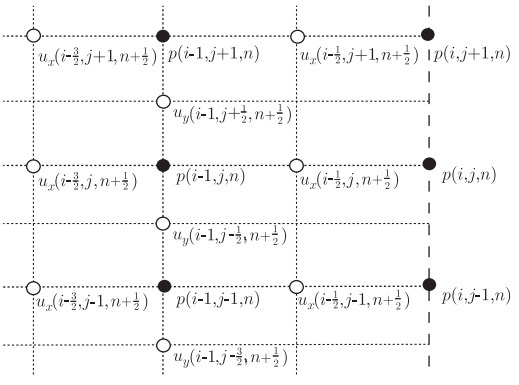


Fig. 1. Acoustic Yee unit cell in FDTD algorithm.

$$u_x(i-\tfrac{1}{2},j,n+\tfrac{1}{2}) = u_x(i-\tfrac{1}{2},j,n-\tfrac{1}{2}) - \frac{\Delta t}{\rho_0 \Delta x}[p(i,j,n) - p(i-1,j,n)], \tag{4}$$

$$u_y(i,j-\tfrac{1}{2},n+\tfrac{1}{2}) = u_y(i,j-\tfrac{1}{2},n-\tfrac{1}{2}) - \frac{\Delta t}{\rho_0 \Delta y}[p(i,j,n) - p(i,j-1,n)], \tag{5}$$

where $i$, $j$, and $n$ represent spatial coordinates and time; i.e., $p(x,y,t) = p(i\Delta x, j\Delta y, n\Delta t)$ is written as $p(i,j,n)$.

Eqs. (3)–(5) are updated in time using a *leapfrog scheme* [14]. First, $u$'s at time step $n+\frac{1}{2}$ are computed from $p$'s at time step $n$ and previous $u$'s at time step $n-\frac{1}{2}$. Then, $p$'s at time step $n+1$ are computed from $u$'s at time step $n+\frac{1}{2}$ and previous $p$'s at time step $n$. This process is repeated until the temporal simulation has been completed. Note that the leapfrog scheme does not introduce dissipation and is reversible in time because of its central symmetry in both time and space. It may happen that a scheme built from symmetric and reversible units may lose any appearance of symmetry, but Roe has shown that such a scheme is nevertheless reversible [13].

The spatial and temporal sampling intervals, $\Delta x, \Delta y$, and $\Delta t$, cannot be left to chance. The formula that ensures stability in an FDTD model can be found by means of Von Neumann's criteria and is known as the Courant condition [14],

$$c\Delta t \leqslant \frac{1}{\sqrt{(1/\Delta x)^2 + (1/\Delta y)^2}}. \tag{6}$$

## 3. The time-domain impedance problem

To obtain realistic simulations impedance boundary conditions must be incorporated in the model. However, the impedance $Z(\omega)$ is usually defined in the frequency domain,

$$P(\omega) = Z(\omega)\mathbf{U}(\omega)\cdot\mathbf{n}, \tag{7}$$

where $P$ and $\mathbf{U}$ are the Fourier transformed sound pressure and particle velocity, and $\mathbf{n}$ is a unit vector perpendicular to the wall.

To incorporate the effect of the impedance on the discrete model and in order to optimize the algorithms, a model of the impedance in terms of a filter structure can be used. A digital filter with an infinite impulse response (an IIR filter) that approximates the frequency response of the impedance is usually employed. Considering a discrete-time signal representation of the pressure and particle velocity, the relation between them becomes

$$P(\mathrm{e}^{\mathrm{j}\omega}) = \frac{\sum_{n=0}^{N-1} c_n \mathrm{e}^{-\mathrm{j}\omega n}}{1 - \sum_{m=1}^{M-1} d_m \mathrm{e}^{-\mathrm{j}\omega m}} \mathbf{U}(\mathrm{e}^{\mathrm{j}\omega})\cdot\mathbf{n}, \tag{8}$$

where the frequency response of the impedance has been approximated by using an IIR filter. This approximation of the frequency response to an IIR filter is usually carried out using Prony [24] or Yule–Walker [25] algorithms.

The IIR filter structure in the frequency domain has a corresponding equation in the time domain [26]. The equation

$$p(i) = \sum_{n=1}^{N} c_n \mathbf{u}(i-n)\cdot\mathbf{n} - \sum_{m=1}^{M-1} d_m p(i-m), \tag{9}$$

where $t = i\Delta t$, can easily be incorporated in the discrete-time model [7,27]. However, such a method requires storing both the sound pressure and the particle velocities at different time steps as coefficients, which leads to a significant increase of the required computer memory since for each position $N$ particle velocity and $M-1$ pressure data points at the boundary cells must be stored from previous time steps.

Furthermore, using such a function in a recursive convolution or using differential methods can be very time-consuming (see Ref. [6] for a detailed comparison of such methods). Moreover, this modifies the FDTD equations (Eqs. (3)–(5)); it can be complicated to obtain a general expression for an indeterminate number of coefficients; and stability is not easy to ensure.

These considerations lead to the conclusion that implementation of an FDTD simulation incorporating frequency dependent boundary conditions will require significant computer resources.

The purpose of this work is to find a simple and stable method of incorporating frequency dependent boundary conditions in an FDTD model. The impedance model is approached using a rational form expressed as a digital filter (independent of the FDTD equations), and by defining an interaction model, mesh and boundary conditions are coupled without modifying the fundamental FDTD algorithm. A direct coupling between mesh and boundary conditions would involve the output of one model being the input to the other and vice versa. To incorporate a digital filter directly makes it possible to use the highly efficient structures of IIR filters. For example, as mentioned above, Eq. (9) requires storing $N+M-1$ values for each boundary cell, but if the filter is incorporated directly it is only necessary to store $N$ values (i.e., using Direct Form II [26] and assuming $N=M$). With the proposed method, the potential of computationally efficient digital filters can be used to reduce the cost of the entire algorithm.

However, such an implicit solution is potentially unstable [28]. To avoid such effects, a method based on the *mixing modelling strategy* is proposed.

## 4. Mixing modelling strategy

If the initial boundary value problem involves coupled domains, each with its own partial differential equation, each such equation can be solved separately. Assuming a seamless transition from one domain to the other, there has to be a function that solves the global system of equations in the combined region and couples it to the boundaries. The so-called *mixing modelling strategy* seems to be a good candidate [8]. All points on the interface between the domains are arranged in pairs of "port variables" representing incoming and outgoing variables. Petrausch et al. [29] have proposed to define a common interaction between the different paradigms (for the 1D case), based on WDFs [9]. In this way the the coupling between adjacent domains or between an interior space and its boundaries becomes a local phenomenon, realized as local communication between two "WDF ports".

### 4.1. Wave digital filters

WDF is an elegant and efficient method for describing continuous networks in the discrete-time domain [9]. The main advantage of WDF is the discretization process. The discretization is carried out separately for each network element by a bilinear transformation [26]. First, the variables $\mathbf{y}(n)$ and $\mathbf{v}(n)$ corresponding to some physical variables are defined. They are known as the *Kirchhoff variables*. Originally, Fetweiss defined these variables as voltage ($\mathbf{y}(n)$) and current ($\mathbf{v}(n)$) [9], but using the *impedance analogy* [30], they can be identified as sound pressure and acoustic particle velocity, respectively. The interaction between this class of variables can give rise to potential computational problems, e.g., delay-free loops or potentially unstable implicit equations.

The delay-free loop problem is a computational handicap in the implementation of discrete systems. Basically, it occurs when the computation of some values requires knowledge of the same value. A digital structure with delay-free loops is physically impossible to achieve due to the finite time required to carry out all arithmetic operations on a computer. And this is what occurs when the FDTD mesh and digital filter are coupled: the input of the filter needs information of the pressure and particle velocity in the boundary cells; and at the same time, these boundary cells need to know the output of the filter.

However, these instabilities can be avoided by introducing the so-called *wave variables*,

$$\mathbf{a}(n) = \mathbf{y}(n) + R\mathbf{v}(n), \tag{10}$$

$$\mathbf{b}(n) = \mathbf{y}(n) - R\mathbf{v}(n). \tag{11}$$

The variables $\mathbf{a}(n)$ and $\mathbf{b}(n)$ represent the outgoing and incoming wave variables, respectively, and propagation information is inherent in them. This transition from the Kirchhoff variables to the wave variables is a key point of the WDF theory, and their capability of avoiding potential instabilities has been widely analysed in the literature [9]. By a proper choice of the "port resistance" $R$, WDFs offer the possibility of separating the design of the block elements from the definition of their interaction by appropriate adaptor elements (see Ref. [29] for details). Note that both in the electrical and the acoustic case, $R$ has the dimensions of an impedance.

The separation and interaction in WDF terms ensure an unconditionally stable model when both parts (the FDTD model of the sound field and the digital filter representation of the impedance) are independently stable. The only source of instability, an implicit equation, is avoided using this variable conversion. A complete review of this issue can be found in Refs. [9,31].

### 4.2. Coupling between FDTD and WDFs

In this section, an FDTD decomposition into WDF is presented. It involves determining incoming and outgoing wave components at interface points of the FDTD simulations. In order to integrate Eqs. (10) and (11) into an FDTD algorithm, $\mathbf{y}(n)$ and $\mathbf{v}(n)$ are identified as the sound pressure and the particle velocity. Thus in the discrete-time domain Eqs. (10) and (11) become

$$\mathbf{a}(i,j,n) = \mathbf{I}p(i,j,n) + R\mathbf{u}(i,j,n), \tag{12}$$

$$\mathbf{b}(i,j,n) = \mathbf{I}p(i,j,n) - R\mathbf{u}(i,j,n), \tag{13}$$

where $\mathbf{I}$ is the identity matrix. Note that $\mathbf{a}$ and $\mathbf{b}$ are vectors with dimensions as the pressure. In a 1D sound field Eqs. (12) and (13) would, with $R = \rho_0 c$, provide a "true" decomposition into two plane waves travelling in opposite direction; here $\mathbf{a}$ and $\mathbf{b}$ represent "incoming" and "outgoing" wave field components in a more loose sense. In the multidimensional case $R$ does not correspond to the physical characteristic impedance of the medium; it must be calculated in order to achieve this wave decomposition, as will be shown later.

The scope is to find a WDF decomposition at the interface point $\mathbf{s}_s = [i_s, j_s]$ in the incoming and outgoing components, where the sound pressure and the particle velocity components at $\mathbf{s}_s$ are unknown at the actual time step. These values depend on neighbouring values of the pressure and the particle velocity calculated using the FDTD algorithm. They are found by means of the FDTD discretized version of the Euler equation, Eq. (2).

As an example, a surface interface with a normal vector in the $x$-direction component is considered. Let the medium be at $i < i_s$. The goal is to find $p(i_s, j_s, n)$ and $u_x(i_s, j_s, n)$ by means of $b_x(i_s, j_s, n)$ and $a_x(i_s, j_s, n)$, using Eqs. (12) and (13). The particle velocity component $u_x(i,j,n)$ cannot be obtained directly from the FDTD scheme due to the staggered distribution of the variables, situated at $(i \pm \frac{1}{2}, j \pm \frac{1}{2}, n \pm \frac{1}{2})$. One possibility could be to determine this quantity as a temporal and spatial average of surrounding and previous points; cf. Eq. (4). However, although this approach would seem to be reasonable, a set of different approximations of $u_x(i,j,n)$ have been implemented and compared, and the results show that case where the medium is at $i < i_s$, the approximating $u_x(i,j,n)$ by $u_x(i - \frac{1}{2}, j, n + \frac{1}{2})$ is a better solution. In case the medium is at $i > i_s$, $u_x(i,j,n) \simeq u_x(i + \frac{1}{2}, j, n + \frac{1}{2})$ should be used.

First $b_x(i_s, j_s, n)$ is calculated. Note that the outgoing component depends on the pressure and the particle velocity at the interface at the present time step, but still remains unknown. In the $x$-direction, Eq. (4) is used. Solving for the pressure gives

$$p(i_s, j_s, n) = p(i_s - 1, j_s, n) - \rho_0 \frac{\Delta x}{\Delta t}\left(u_x\left(i_s - \frac{1}{2}, j_s, n + \frac{1}{2}\right) - u_x\left(i_s - \frac{1}{2}, j_s, n - \frac{1}{2}\right)\right). \tag{14}$$

Inserting Eq. (14) into Eq. (12) gives, with $R = \rho_0 \Delta x / \Delta t$,

$$b_x(i_s, j_s, n) = p(i_s - 1, j_s, n) - R \cdot u_x(i_s - \tfrac{1}{2}, j_s, n - \tfrac{1}{2}). \tag{15}$$

This particular value of $R = \sqrt{2}\rho_0 c$ with $c\Delta t = \Delta x/\sqrt{2}$ (cf. the Courant condition, Eq. (6)) ensures that the outgoing component depends only on previous and known values of the pressure and the particle velocity and not on the boundary condition. The incoming component is obtained as the outgoing component in the other

block. It is assumed that $a_x(i_s,j_s,n)$ is known. Once the wave variables at interface points are known, Eqs. (12) and (13) are used to obtain both the pressure and the particle velocity at these points at instant $n$. The same process is necessary for calculating the $y$-component.

The approach used for the spatial average of the particle velocity introduces some errors (undesirable reflections). One way of reducing these errors would be to use a more accurate approximation of the finite differences in the Euler equation. A third-order finite-difference approximation provides a good trade-off between accuracy and computational cost [23]

$$p(i_s,j_s,n)=\frac{4}{3}p(i_s-1,j_s,n)-\frac{1}{3}p(i_s-2,j_s,n)-\rho_0\frac{\Delta x}{\Delta t}\left(u_x\left(i_s-\frac{1}{2},j_s,n+\frac{1}{2}\right)-\frac{4}{3}u_x\left(i_s-\frac{1}{2},j_s,n-\frac{1}{2}\right)+\frac{1}{3}u_x\left(i_s-\frac{1}{2},j_s,n-\frac{3}{2}\right)\right). \tag{16}$$

Following the same procedure used in deriving Eq. (15), the outgoing component is achieved as

$$b_x(i_s,j_s,n)=\frac{4}{3}p\left(i_s-1,j_s,n\right)-\frac{1}{3}p\left(i_s-2,j_s,n\right)-R\left(-\frac{4}{3}u_x\left(i_s-\frac{1}{2},j_s,n-\frac{1}{2}\right)+\frac{1}{3}u_x\left(i_s-\frac{1}{2},j_s,n-\frac{3}{2}\right)\right), \tag{17}$$

with $R=\sqrt{2}\rho_0 c$. The two methods are compared in Section 5.

It should be emphasized that although third-order approaches (and more generally, all approaches of odd order) are dispersive, this approach is only used at the boundary points and does not affect the propagation properties of the FDTD method used to simulate the sound field. The signal/reflection ratio for the second-order finite-differences approach has been measured and it is around −27 dB. However, using the third-order finite-differences approach this ratio has been reduced to about −52 dB.

### 4.3. Interaction between digital filters and WDFs

In the present work, the coupling between digital filters representing the impedance model with WDF ports has been implemented using the model introduced by Petrausch and Rabenstein [32]. Their solution is based on Space State Systems (SSS); see Fig. 2(a).

Consider a digital filter representation of a rational expression of the impedance (Eq. (8)). This digital filter is represented in Fig. 2(b), where $z^{-1}$ represents a unit delay. Any linear system can be expressed in terms of an SSS. In the present case a single input, $u_n(n)=\mathbf{u}(n)\cdot\mathbf{n}$ (the normal component of the particle velocity on the impedance surface), and a single output $p(n)$ (the pressure on the same surface) are related as follows:

$$\mathbf{z}(n+1)=\mathbf{A}\mathbf{z}(n)+\mathbf{B}u_n(n), \tag{18}$$

$$p(n)=\mathbf{C}\mathbf{z}(n)+Du_n(n). \tag{19}$$

The vector $\mathbf{z}(n)$ is the system state ($\mathbf{z}(n)=[z_1(n),z_2(n)]$ in the example shown in Fig. 2(b)). In this case, $\mathbf{A}$ is a matrix, $\mathbf{B}$ and $\mathbf{C}$ are vectors, and $D$ is a scalar (see Ref. [26] for more details).

Delay-free loops in the interconnection of the SSS with WDF (implicit equations) are avoided by the following procedure: Eq. (19) is inserted into Eqs. (12) and (13), and the following system equations are obtained:

$$a(n)=\mathbf{C}\mathbf{z}(n)+(D+R)u_n(n), \tag{20}$$

$$b(n)=\mathbf{C}\mathbf{z}(n)+(D-R)u_n(n). \tag{21}$$

Instantaneous feedback is avoided with $R=D$ since $b(n)$ becomes independent of $u_n(n)$. Thus,

$$u_n(n)=\frac{1}{2D}(a(n)-\mathbf{C}\mathbf{z}(n)), \tag{22}$$

$$b(n)=\mathbf{C}\mathbf{z}(n). \tag{23}$$

As an example, a second-order IIR filter that represents the impedance is adapted to WDF ports; see Fig. 2(b). According to space state theory, a second-order IIR digital filter is represented as an SSS by the

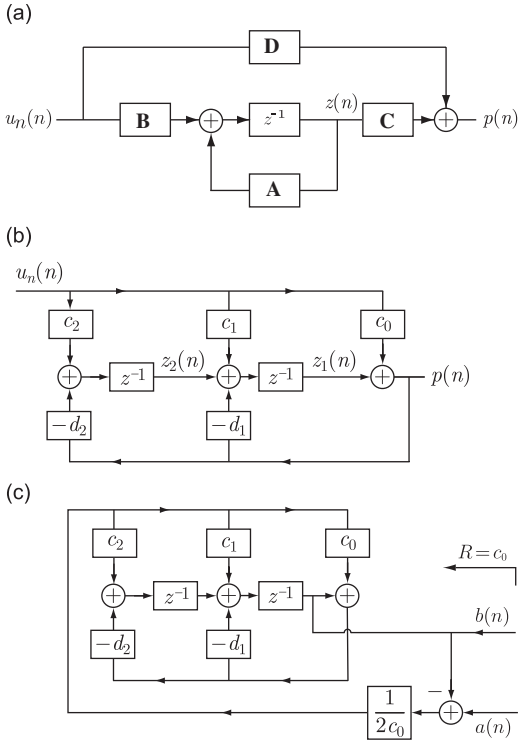


Fig. 2. (a) Discrete state-space description of a linear system. (b) Second-order discrete system in observable canonical form. (c) Interaction of a second-order IIR filter with WDF ports.

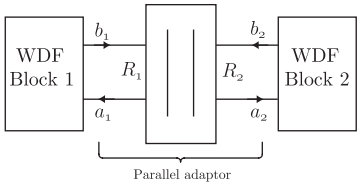


Fig. 3. Interconnection of WDFs using an adaptor.

following equations:

$$\mathbf{z}(n+1) = \begin{pmatrix} -c_1 & 1 \\ -c_0 & 0 \end{pmatrix} \mathbf{z}(n) + \begin{pmatrix} d_1 - d_2 c_1 \\ d_0 - d_2 c_0 \end{pmatrix} u_n(n),$$

$$p(n) = \begin{pmatrix} 1 & 0 \end{pmatrix} \mathbf{z}(n) + d_2 \cdot u_n(n). \tag{24}$$

The digital filter that represents the impedance realized with WDF ports is shown in Fig. 2(c).

### 4.4. Coupled model

In the coupled model, each block see the other block as a WDF port. In order to couple two WDFs and avoid instabilities, it is necessary to use a two-port parallel adaptor to adapt the impedance and avoid direct feedback loops; see Fig. 3. This adaptor (known as *parallel adaptor* in the WDF literature [28]) relates

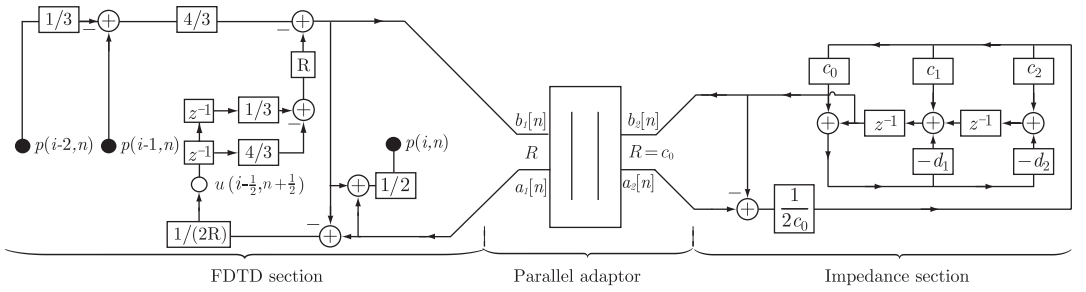


Fig. 4. Complete model of the proposed implementation by using a second-order approach. FDTD mesh and the impedance digital filter are implemented separately. A two-port parallel adaptor connects the two models.

wave variables with different impedance ports. A matrix description for a parallel adaptor of two WDFs, 1 and 2, is

$$\begin{pmatrix} a_1 \\ a_2 \end{pmatrix} (R_1 + R_2)^{-1} \begin{pmatrix} R_2 - R_1 & 2R_1 \\ 2R_2 & R_1 - R_2 \end{pmatrix} \begin{pmatrix} b_1 \\ b_2 \end{pmatrix}. \tag{25}$$

Once the interaction between the models has been specified, the frequency dependent FDTD model shown in Fig. 4 results.

## 5. Results

Some simulations have been carried out in order to examine the performance of the proposed method of realizing a frequency dependent impedance boundary condition. Examples in 1D and 2D are presented. The impedance model selected for these experiments is that of a hard-backed layer of porous material with a thickness $d$ [33],

$$Z(\omega) = -\mathrm{j}Z_p(\omega)\cot(k_p(\omega)d), \tag{26}$$

where the material is modelled using Delany and Bazley's empirical one-parameter model [34], that is, the characteristic impedance and wavenumber of the material are given by

$$Z_p(\omega) = \rho_0 c(1 + 0.057X^{-0.754} - \mathrm{j}0.087X^{-0.732}), \tag{27}$$

$$k_p(\omega) = \rho_0 c(1 + 0.098X^{-0.7} - \mathrm{j}0.189X^{-0.595}), \tag{28}$$

where $X = \rho_0\omega/(2\pi\sigma)$ and $\sigma$ is the material's flow resistivity.

In what follows a 0.1 m thick layer of porous material with a flow resistivity of 1000 kg $\mathrm{m}^{-3}\mathrm{s}^{-1}$ is considered. The coefficients of the digital filter are determined from the analytical expression of the impedance using a Prony algorithm and an IIR digital filter of 40th order. The performance of the FDTD model is examined by determining the plane wave reflection factor $R(\omega,\theta)$ [33],

$$R(\omega,\theta) = \frac{Z(\omega)\cos\theta - \rho_0 c}{Z(\omega)\cos\theta + \rho_0 c}, \tag{29}$$

where $\theta$ is the angle of incidence of a plane wave.

Note that the impedance spectrum obtained by the digital filter design should be as accurate as possible. Even small differences between the reference impedance and the digital filter design can give rise to significant differences between the physical (or theoretical) reflecting factor and the one obtained by the digital impedance.

All the FDTD results presented here are based on a homogeneous discretization, with $\Delta x = \Delta y$. The sampling frequency is 40 kHz, and the source is a Ricker wavelet with a bandwidth of $W = f_s/8$ (this means 8 grid points per wavelength). These values have been selected in order to minimize the effects of dispersion. The spatial sampling has been determined from the Courant condition (Eq. (6)). In order to avoid reflections from

the other walls than the one under test, absorbing boundary conditions have been implemented. In these cases, a Perfect Matched Layer [35] boundary condition has been chosen. It should finally be mentioned that the influence of the mesh has been tested and shown to be negligible.

The FDTD model is tested by determining the reflection factor and comparing with the analytical expression result based on a locally reacting impedance. The first test case is a 1D simulation where one side contains an absorbing boundary condition and the other one the impedance model. The spatial sampling has been selected assuming equality in the Courant condition (Eq. (6)) and in the 1D case, the results are free of dispersion. The results are shown in Fig. 5. As mentioned in Section 4.2, better accuracy can be obtained by increasing the order of the finite differences in the Euler equation. Fig. 5 compares the analytical solution with two different FDTD solutions determined using a second-order and a third-order approach. It can be seen that the third-order approach provides results in best agreement with the analytical reflecting factor; the maximum error of the third-order approach is about 0.3 dB.

The next results have been determined using a 2D FDTD grid. In this case the mesh follows the scheme presented in Section 4.2, and the Perfect Matched Layer algorithm is used for the absorbing boundaries, as in the 1D case. It is interesting to compare the dependence of the angle of incidence with the behaviour of the locally reacting model. In order to determine the reflection factor in the 2D mesh a point source and an observation point are arranged such that the angle of incidence can be varied. The point source has been placed sufficiently far from the impedance surface for the plane wave reflection factor to be indistinguishable from the spherical reflection factor [36]. The difference between the incident and reflected spectrum must be compensated for geometrical propagation losses; in the 2D case this is $1/\sqrt{r}$.

It can be seen that the results shown in Fig. 6 (continuous line) are similar to the analytical solution (dashed line) at all angles (0°, 15°, 30°, 45°, 60°, and 75°). However, there are also some deviations. The differences are partly due to the angle dependent artificial dispersion of the FDTD method [37] (even though the frequencies have been selected for minimal dispersion effects); this effect can be observed in Fig. 6(d), which corresponds to an angle of incidence of 45°, and the error is very small (in the FDTD mesh used here, this is the angle with no dispersion). However, the most significant source of error is due to the WDF approach in the FDTD mesh as described in Section 4.2: undesirable reflections can appear depending on the incident waveform. Because of such reflections some differences between theoretical and observed reflection factor levels occur. The maximum difference can be seen to be about 1 dB in most of the results; however, somewhat larger differences are observed in Fig. 6(e), which corresponds to angle of incidence of 75°, particularly in the dips.

It is worth emphasizing that the results follow a locally reacting model without any artificial modification of the boundary condition filter. This is due to the use of the impedance expression directly in the simulation. Thus, a digital filter implementation of the reflecting factor [38,39], similar to the method based on digital waveguide mesh [40,41], is avoided. The reflecting factor, Eq. (29), depends on the angle of incidence, and

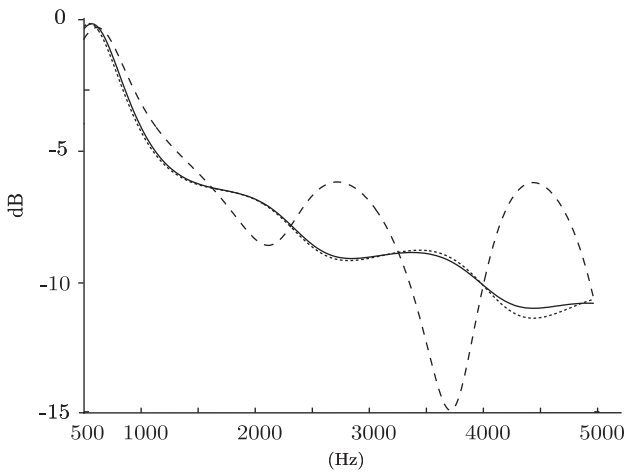


Fig. 5. FDTD reflecting factor calculated with a 1D mesh. The continuous line represents the reflecting factor obtained with a third-order approach; the dashed line is the reflecting factor obtained with a second-order approach and the dotted line is the theoretical result.

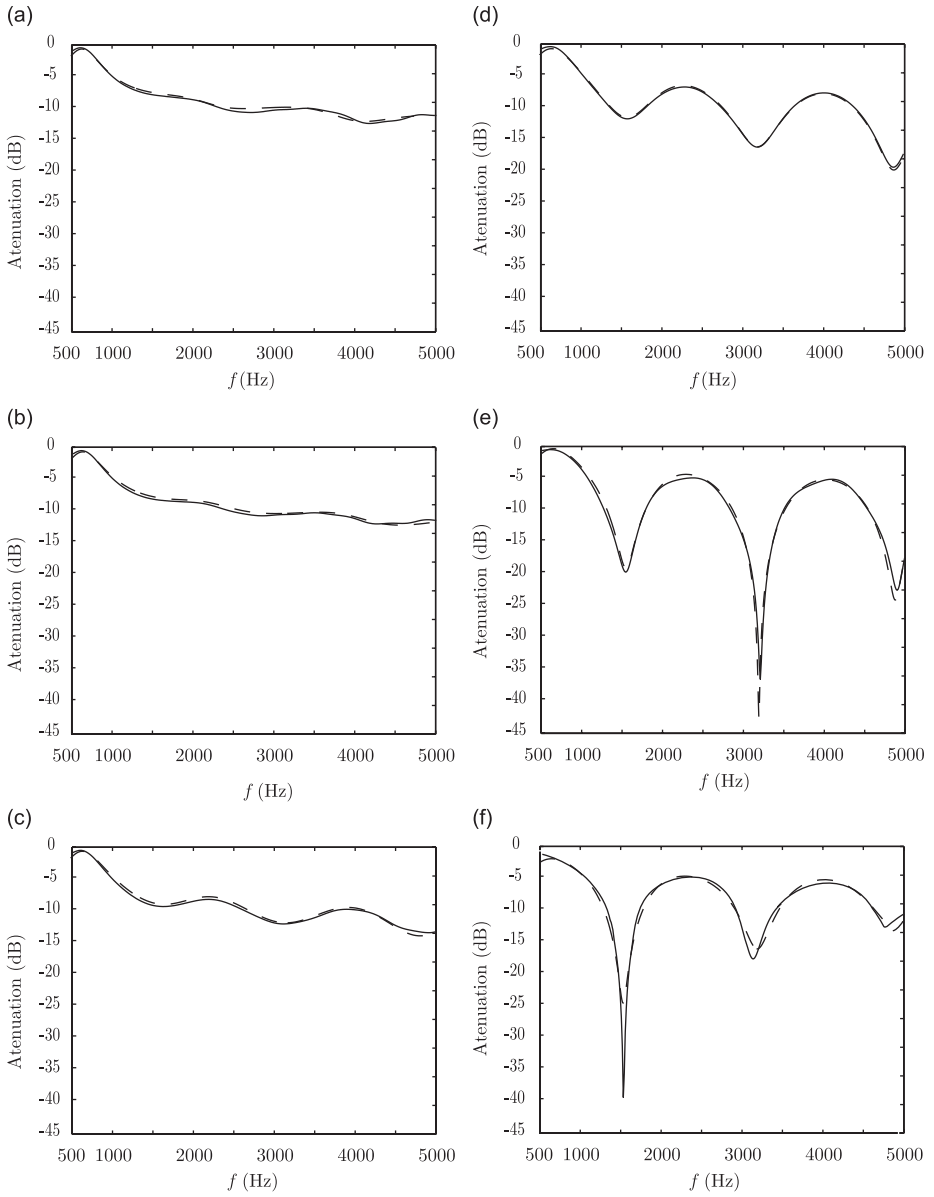


Fig. 6. FDTD reflecting factor calculated with a 2D mesh (continuous line), compared with the theoretical reflecting factor (dashed line), for the angles: (a) 0°, (b) 15°, (c) 30°, (d) 45°, (e) 60°, (f) 75°.

therefore it would be necessary to calculate it in each iteration to obtain the appropriate locally reacting model [42]. The proposed solution therefore represents a considerable reduction of the computational cost and a comparatively higher efficiency based on hybrid models between FDTD and the digital waveguide mesh.

So far the model has been tested in an idealized situation where one single plane wave is incident on an impedance wall. However, in realistic situations several plane waves may well be incident simultaneously. In Fig. 7, a case where two simultaneous plane wave strikes the impedance surface at angles $\alpha_1 = 30^\circ$ and $\alpha_2 = 60^\circ$ is shown.

In order to validate the linearity of the proposed method, three simulations are carried out, two in which the two plane waves are launched separately, and a third one where the two plane waves are incident at the same time. Two kinds of analysis are carried out: one related with the reflecting factor and another one related with the impulse responses.

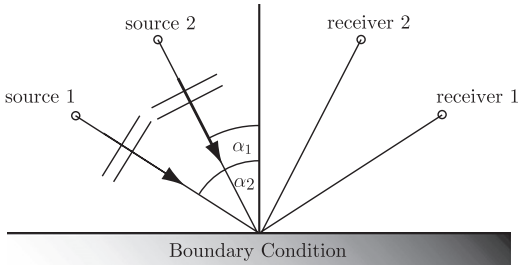


Fig. 7. Set-up used for analysing the linearity of the proposed method.

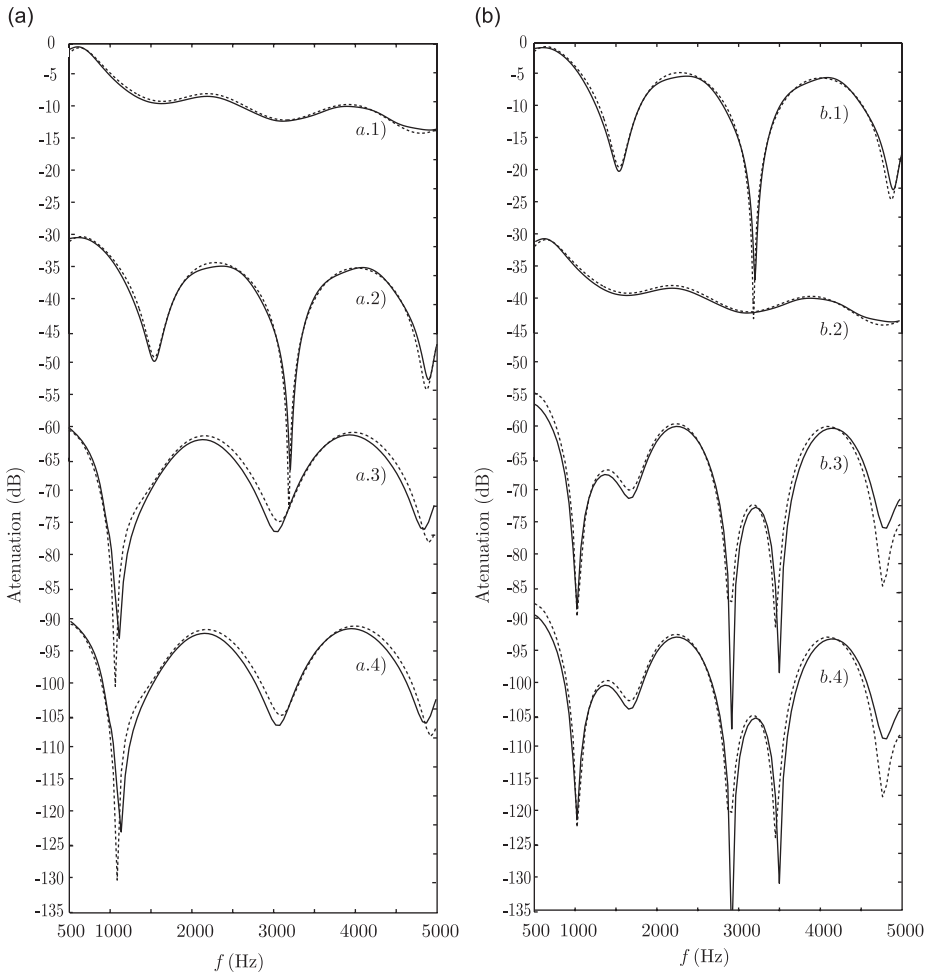


Fig. 8. Spectrum of the reflecting factor obtained in the simulation (continuous lines) versus theoretical results (dotted lines): (a) at receiver 1—(a.1) with plane wave at $\alpha_1 = 30^\circ$, (a.2) with plane wave at $\alpha_2 = 60^\circ$, (a.3) both plane waves at the same time, (a.4) adding both separated plane waves; (b) at receiver 2—(b.1) with plane wave at $\alpha_2 = 60^\circ$, (b.2) with plane wave at $\alpha_1 = 30^\circ$, (b.3) both plane waves at the same time, (b.4) adding both separated plane waves. Each spectrum is shifted −30 dB.

First the results are analysed in the frequency domain. In Fig. 8(a), the results at receiver 1 appear (see Fig. 7). In all the presented spectra the results from the simulations (continuous lines) are compared with the expected theoretical results (dotted lines). Fig 8(a.1) shows the spectra when only the plane wave at $\alpha_1 = 30^\circ$ is emitted, and Fig 8(a.2) shows the spectra with the plane wave at $\alpha_2 = 60^\circ$. These results are identical to the results shown in Figs. 6(c) and (d) and agree very well with the theoretical results. Fig. 8(a.3) shows the spectra

that result when both plane waves strike the boundary at the same time. The linearity is demonstrated when the result is compared with Fig. 8(a.4), that is, the result obtained if both independent plane waves are added (Figs. 8(a.1) and (a.2)). Comparing Figs. 8(a.3) and (a.4) shows that there is no difference between them. This confirms the linearity of the proposed method.

In the time domain the same procedure has been followed. However, the impulse responses waveform is more sensitive to the inherent dispersion (in that case, to the angle dependent dispersion). For this reason, the impulse responses represented in Fig. 9 have been represented following a minimum-phase consideration (which means that they have the same magnitude response as the original systems; however, the energy is concentrated near the start of the impulse responses and they have minimum group delay) and only delays relative to the time difference of arrival have been taken into account; possible effects of the FDTD mesh angular dispersion are not considered in this time-domain analysis. It can be seen that there is no significant difference between the results and the expected theoretical results. The comparison between the results when

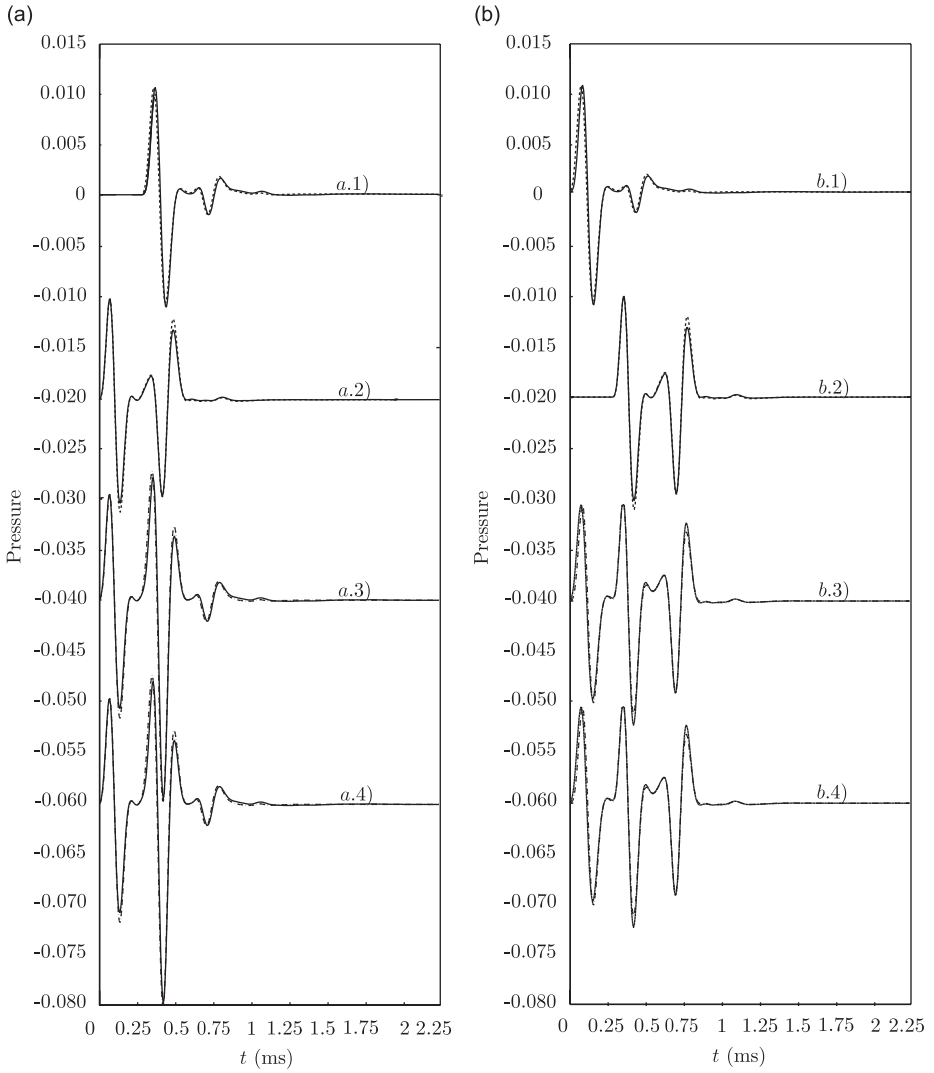


Fig. 9. Impulse responses obtained in the simulation (continuous line) versus theoretical results (dotted line): (a) at the receiver 1—(a.1) with plane wave at $\alpha_1 = 30^\circ$, (a.2) with plane wave at $\alpha_2 = 60^\circ$, (a.3) both plane waves at the same time, (a.4) adding both separated plane waves; (b) at receiver 2—(b.1) with plane wave at $\alpha_2 = 60^\circ$, (b.2) with plane wave at $\alpha_1 = 30^\circ$, (b.3) both plane waves at the same time, (b.4) adding both separated plane waves. Each impulse response is shifted −20 mPa.

the two plane waves appear at the same time and the result of adding the corresponding separate results demonstrates again the linear behaviour: there is no difference between the results.

## 6. Conclusions

A new method of incorporating frequency dependent absorbing boundary conditions in an FDTD model has been proposed. In this model, the FDTD mesh and the boundary conditions (an impedance model defined by means of a digital filter) are implemented separately and joined using an interface based on WDF. The advantage of the method is that stability is ensured if both elements are separately stable, because of delay-free loops (implicit equations) are avoided. Another important feature is that the definition of the digital filter can be designed with highly efficient structures, reducing considerably the computational cost of the whole algorithm; and even allowing to modify the coefficients and the order of the filter without affecting the algorithm during the execution of the code. The proposed method is able to model a locally reacting impedance without introducing any substantial increase of the computational cost.

## Acknowledgements

José Escolano's stay at DTU has been made possible by a Marie Curie scholarship from the EC. The work of José J. López has been supported by Spanish Ministry of Science and Technology (MCYT) under Project ref. TEC2006-13883-C04-01 and FEDER funds.

## References

[1] D. Botteldooren, Finite-difference time-domain simulation in a quasi-Cartesian grid, *Journal of the Acoustical Society of America* 95 (1994) 2313–2319.
[2] D. Botteldooren, Finite-difference time-domain simulation of low-frequency room acoustic problems, *Journal of the Acoustical Society of America* 98 (1995) 3302–3308.
[3] J. Lovetri, D. Mardare, G. Soulodre, Modeling of the seat dip effect using the finite-difference time-domain method, *Journal of the Acoustical Society of America* 100 (1996) 2204–2212.
[4] H. Dong, A.M. Kaynia, C. Madshus, J.M. Hovem, Sound propagation over layered poro-elastic ground using a finite-difference model, *Journal of the Acoustical Society of America* 108 (2000) 494–502.
[5] K.Y. Fung, H. Ju, Time-domain impedance boundary conditions for computational acoustics and aeroacoustics, *Journal of Computational Fluid Dynamics* 18 (2004) 503–511.
[6] D.M. Sullivan, A frequency-dependent FDTD method using $Z$ transforms, *IEEE Transactions on Antennas and Propagation* 40 (1992) 1223–1230.
[7] K. Heutschi, M. Horvath, J. Hofmann, Simulation of ground impedance in finite difference time domain calculations of outdoor sound propagation, *Acta Acustica united with Acustica* 91 (2005) 35–40.
[8] M. Karjalainen, C. Erkut, L. Savioja, Compilation of unified physical models for efficient sound synthesis, *International Conference on Acoustics, Speech and Signal Processing (ICASSP'03)*, Hong Kong, China, 2003.
[9] A. Fettweis, Wave digital filters: theory and practice, *Proceeding of the IEEE* 74 (1986) 270–327.
[10] K.S. Yee, Numerical solution of initial boundary value problems involving Maxwell's equations in isotropic media, *IEEE Transactions on Antennas and Propagation* 14 (1966) 302–307.
[11] J.G. Maloney, K.E. Cummings, Adaptation of FDTD techniques to acoustic modelling, *11th Annual Review of Progress in Applied Computational Electromagnetics*, Vol. 2, Monterey, CA, USA, 1995, pp. 724–731.
[12] J. P. Thomas, An Investigation of the Upwind Leapfrog Method for Scalar Advection and Acoustic/Aeroacoustic Wave Propagation Problems, *PhD Thesis*, University of Michigan, Ann Arbor, MI, 1996.
[13] P. Roe, Linear bicharacteristic schemes without dissipation, *SIAM Journal on Scientific Computing* 19 (5) (1998) 1405–1427.
[14] A. Taflove, *Computational Electromagnetics*, Artech House, Boston, MA, 1995.
[15] L. Savioja, T. J. Rinne, T. Takala, Simulation of room acoustics with a 3-D finite difference mesh, *Proceedings of the International Computer Music Conference (ICMC'94)*, Aarhus, Denmark, 1994, pp. 463–466.
[16] J. Escolano, J.J. López, B. Pueo, Directive sources in acoustic discrete-time domain simulations based on directivity diagrams, *Journal of the Acoustical Society of America* 121 (6) (2007) EL256–EL262.
[17] A. Chaigne, A. Askenfelt, Numerical simulations of piano strings—Part I: a physical model for a struck string using finite difference methods, *Journal of the Acoustical Society of America* 95 (2) (1994) 1112–1118.
[18] J. Bensa, S. Bilbao, R. Kronland-Martinet, J.O. Smith, The simulation of piano string vibration: from physical models to finite difference schemes and digital waveguides, *Journal of the Acoustical Society of America* 114 (2) (2003) 1095–1107.

[19] M. Karjalainen, C. Erkut, Digital waveguides vs. finite difference schemes: equivalence and mixed modeling, *EURASIP Journal on Applied Signal Processing* 2004 (2004) 978–989.
[20] L. Liu, D. Albert, Acoustic pulse propagation near a right-angle wall, *Journal of the Acoustical Society of America* 119 (4) (2006) 2073–2083.
[21] D. Botteldooren, Time-domain simulation of the influence of close barriers on sound propagation to the environment, *Journal of the Acoustical Society of America* 101 (1997) 1278–1285.
[22] V. Ostashev, D. Wilson, L. Liu, D. Aldridge, N. Symons, D. Marlin, Equations for finite-difference time-domain simulation of sound propagation in moving inhomogeneous media and numerical implementation, *Journal of the Acoustical Society of America* 117 (2005) 503–517.
[23] J. Strikwerda, *Finite Difference Schemes and Partial Differential Equations*, Wadsworth and Brooks/Cole, Pacific Grove, CA, USA, 1989.
[24] T.W. Parks, C.S. Burrus, *Digital Filter Design*, Wiley, New York, 1987.
[25] B. Friedlander, B. Porat, The Modified Yule–Walker Method of ARMA spectral estimation, *IEEE Transactions on Aerospace Electronic Systems* 20 (2) (1984) 158–173.
[26] J.G. Proakis, D.G. Manolakis, *Digital Signal Processing*, third ed., Prentice Hall International, NJ, USA, 1996.
[27] Y. Özyörük, L.N. Long, A time-domain implementation of surface acoustic impedance condition with and without flow, *Journal of Computational Acoustics* 5 (1997) 277–296.
[28] S. Bilbao, *Wave and Scattering Methods for the Numerical Integration of Partial Differential Equations*, Wiley, New York, 2004.
[29] S. Petrausch, J. Escolano, R. Rabenstein, A general approach to block-based physical modeling with mixed modeling strategies for digital sound synthesis, *International Conference on Acoustics, Speech and Signal Processing (ICASSP'05)*, Philadelphia, USA, 2005.
[30] L.L. Beranek, *Acoustics, Acoustical Society of America*, American Institute of Physics, Woodbury, NY, USA, 1993.
[31] A. Fettweis, Pseudopassivity, sensitivity, and stability of wave digital filters, *IEEE Transactions on Circuit Theory* 19 (1972) 668–673.
[32] S. Petrausch, R. Rabenstein, Interconnection of state space structures and wave digital filters, *IEEE Transactions on Circuits and Systems II* 52 (2004) 90–93.
[33] H. Kuttruff, *Room Acoustics*, fourth ed., Spon Press, New York, 2000.
[34] M.E. Delany, E.N. Bazley, Acoustical properties of fibrous absorbents materials, *Applied Acoustics* 3 (1970) 105–116.
[35] X. Yuan, D. Borup, J.W. Wiskin, M. Berggren, R. Eidens, S.A. Johnson, Formulation and validation of Berenger's PML absorbing boundary for the FDTD simulation of acoustic scattering, *IEEE Transactions on Ultrasonics, Ferroelectrics and Frequency Control* 44 (1997) 816–822.
[36] P.A. Butov, Reflection of a spherical wave from an impedance boundary, *Soviet Physical Acoustics* 27 (1981) 191–193.
[37] A. Taflove, Review of the formulation and applications of the finite-difference time-domain method for numerical modeling of electromagnetic wave interaction with arbitrary structures, *Wave Motion* 10 (1998) 547–582.
[38] J. Huopaniemi, L. Savioja, M. Karjalainen, Modelling of reflections and air absorption in acoustical spaces—a digital filter design approach, *Proceedings of the IEEE Workshop on Applications of Signal Processing to Audio and Acoustics (WASPAA'97)*, New York, USA, 1997.
[39] D.T. Murphy, M. Beeson, The KW-boundary hybrid digital waveguide mesh for room acoustics applications, *IEEE Transactions on Audio, Speech and Language Processing* 15 (2) (2007) 552–564.
[40] S.A. Van Duyne, J. O. Smith, Physical modeling with the 2-D digital waveguide mesh, *Proceedings of the 1993 International Computer Music Conference*, Tokyo, Japan, 1993, pp. 40–47.
[41] L. Savioja, J. Huopaniemi, T. Lokki, R. Vaananen, Creating interactive virtual acoustic environments, *Journal of the Audio Engineering Society* 47 (9) (1999) 675–705.
[42] J. Escolano, F. Jacobsen, A note on the physical interpretation of frequency dependent boundary conditions in a digital waveguide mesh, *Acta Acustica united with Acustica* 93 (3) (2007) 398–402.